Control of bidirectional physical human–robot interaction based on the human intention

Paulo Leica, Flavio Roberti, Matías Monllor, Juan M. Toibero & Ricardo Carelli

Intelligent Service Robotics

ISSN 1861-2776
Volume 10
Number 1

Intel Serv Robotics (2017) 10:31-40
DOI 10.1007/s11370-016-0207-4

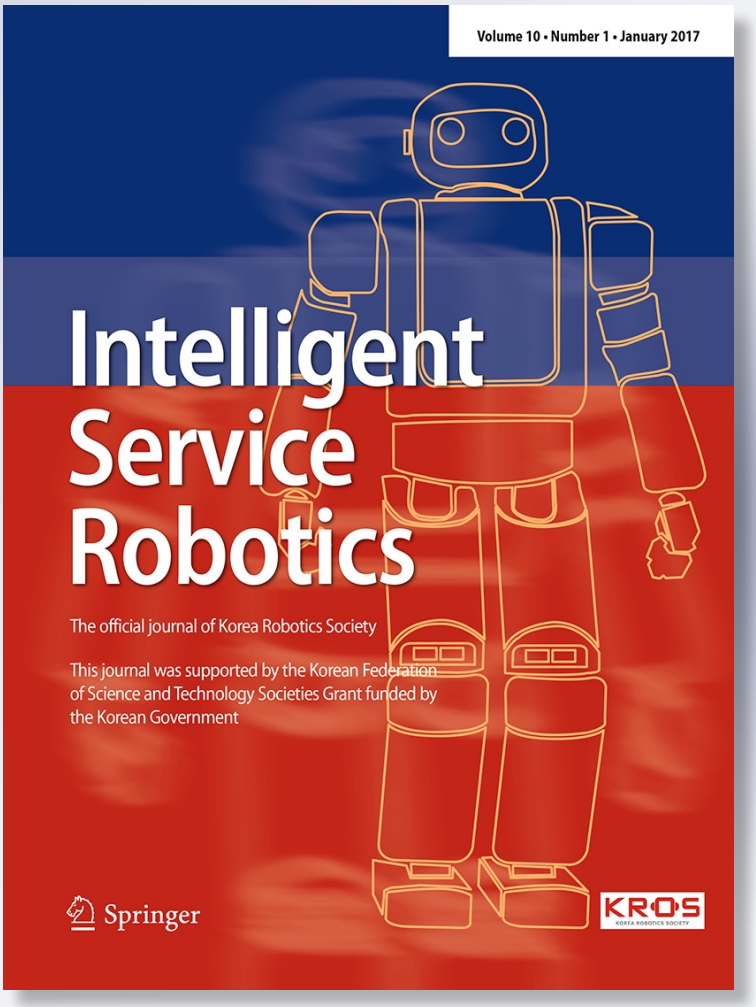

Springer

Intel Serv Robotics (2017) 10:31–40
DOI 10.1007/s11370-016-0207-4

ORIGINAL RESEARCH PAPER

Control of bidirectional physical human–robot interaction based on the human intention

Paulo Leica[1] · **Flavio Roberti**[2] · **Matías Monllor**[2] · **Juan M. Toibero**[2] · **Ricardo Carelli**[2]

Received: 13 April 2016 / Accepted: 18 September 2016 / Published online: 24 September 2016

Abstract This paper presents a control strategy for human–robot interaction with physical contact, recognizing the human intention to control the movement of a non-holonomic mobile robot. The human intention is modeled by mechanical impedance, sensing the human-desired force intensity and the human-desired force direction to guide the robot through unstructured environments. Robot dynamics is included to improve the interaction performance. Stability analysis of the proposed control system is proved by using Lyapunov theory. Real experiments of the human–robot interaction show the performance of the proposed controllers.

Keywords Robotic · Human–robot interaction · Bidirectional interaction · Impedance · Lyapunov

✉ Flavio Roberti
froberti@inaut.unsj.edu.ar

Paulo Leica
paulo.leica@epn.edu.ec

Matías Monllor
mmonllor@inaut.unsj.edu.ar

Juan M. Toibero
mtoibero@inaut.unsj.edu.ar

Ricardo Carelli
rcarelli@inaut.unsj.edu.ar

[1] Escuela Politécnica Nacional, Ladrón de Guevara E11-253, Quito, Ecuador

[2] Instituto de Automática, Universidad Nacional de San Juan-Consejo Nacional de Investigaciones Científicas y Técnicas, Av. San Martin Oeste 1109, J5400ARL San Juan, Argentina

1 Introduction

Research efforts have been focused on providing mobile robots the ability to move and interact with a high degree of autonomy in unstructured environments. In current robotic applications, these environments not only involve objects and other robots, but also raise awareness for the need to interact with humans. This interaction with humans can be justified by the following objectives: (1) the robot can move safely and independently in a human–robot environment to perform a specific task or (2) the robot interacts with the human in a safe, friendly way [1], without [2,3] or with physical contact. This last approach has particular interest in this work, specifically related to the interaction with physical contact. In this context, the use of robots operating close to humans for service tasks, assistance to disabled people [4], household tasks, carrying loads, etc., has been intensified in recent years and its generalization is expected in the future. Thus, there is a great need to develop robots for use in daily activities and real environments based on physical interaction with humans. Among these applications, the partial replacement of nurses can be mentioned for the fast-growing elderly population who suffers deficiencies in motor functions and muscle weakness or enhancing activities such as carrying loads through the physical interaction between a human and a robot. It should be noted that, in the practical use of robots with physical interaction, the safety of users must be considered and, thus, tools allowing a safe interaction with the robot must be developed. Therefore, it is necessary to set up robots to help or enhance the daily activities of people safely. In the event of an active robot failure, analysis is required when control of an active robot fails from the security perspective, i.e. when the robot moves involuntarily, potentially endangering humans in the area. Thus, [5] proposes a load-carrying system for passive robots in cooperation with a human including obstacle avoid-

ance. Similarly, [6] shows a control for passive robots to transport objects based on braking control for object avoidance. In [7], a load-carrying system is proposed with a free arm to reduce human force. Robots with contact in the area of physical support and personal services have been developed in [8]. A walker based on passive robotics to assist the elderly, handicapped people, and the blind was proposed in [9]. The personal aid for the mobility and monitoring system to provide mobility assistance was proposed in [10]. Robotic system as personal service robots for the elderly and disabled was developed [11]. Thus, studies such as [12] show the cooperation in transporting objects using non-holonomic mobile robots without considering human force. Most of the works focus on solving these problems with passive robots due to the security that they represent. However tasks such as load transport, robot guidance along a path with slopes, or the guiding of robots with large inertia may require greater physical effort. References [13,14] show the physical interaction for the transporting objects between mobile manipulators and a human; however in these works, the human should apply a large force during all interactions.

Another area of interest is the recognition of human intention. It becomes relevant in rehabilitation areas where walkers, guiding visually impaired people or carrying loads by handicapped persons or the elderly are used. Reference [15] shows a system that controls the movement of a passive robot, considering the human intention based on the force applied in the direction of the movement. Similarly, [16] presents a physical interaction to guide a robot through a semi-structured environment by means of a force, whereas [17] shows a robot–human physical interaction to guide a robot which is capable of learning the desired path. A robot that interacts with people and interprets human behavior was proposed in [18]. Also, a foot support system which contemplates the human intention is presented in [19]. A manufacturing system that is controlled based on the human intention was proposed in [20]. The motion control of omnidirectional robots based on human intention was proposed in [21]. Also under this point of view, [22] proposed a controller which considers the human intention, to mitigate the negative effects produced by possible visual distractions of the user when he drives a car-like robot. References [23,24] show robotic systems for people guiding and fall prevention based on the human intention. The dance partner robot, which estimates the intention of the human dancer, was proposed in [25,26].

This paper proposes to work with robots equipped with servo motors to enhance the force generated by the human on the robot in tasks such as object transportation or guiding people with an easy and comfortable movement of the robot along the environment. From the robot control system standpoint, the human intention provides a reference trajectory in real time for the robot motion controller such that a good performance in the robot control can be obtained. Therefore, in this work, a control strategy is developed for bidirectional robot–human interaction with contact, based on human intention for motion control of a non-holonomic mobile robot. The authors aim to determine the velocity induced by the human force, hereinafter called as u_{VIFH}, to control the robot. Specifically, this velocity is modeled using the concept of mechanical impedance, with its inputs being the forces (magnitude and orientation) applied by the human. The objective behind developing these controllers is to allow people to guide the robot through an unknown environment, or assist a person with reduced strength, the elderly, or children to carry heavy loads with minimal effort during the entire interaction. Velocity u_{VIFH} is modeled using mechanical impedance; thus, the person feels the inertia generated by the robot during the entire interaction, along with the virtual force generated by an obstacle avoidance strategy for collision prevention in congested environments. This allows bidirectional interaction between the human and the robot. The obstacle avoidance strategy enables the human to easily guide the robot through doors or narrow places without colliding, which is particularly useful in tasks with visually impaired people. The work not only includes the rigorous mathematical formulation of the control laws with their stability proof, but also experimental results to illustrate the good performance of the proposed control strategy.

The rest of this paper is organized as follows. Section 2 presents the structure of the robot and an approach to the problem. In Sect. 3, the environment forces and the human forces are modeled. Section 4 describes the control laws and the stability analysis based on Lyapunov theory. Section 5 reports the experimental results. Finally, in Sect. 6 the conclusions of the research are presented.

2 Approach to the problem

As noted in Sect. 1, this robot has been developed to be used in tasks such as load carrying, people guiding, or moving the robot along any unstructured environment in an easily and comfortably way. One of the most important robot tasks is to correctly estimate the human intention during the interaction. From the control system point of view, the human intention provides a reference for the robot motion controller. The proposed control strategy will allow a person with limited visual or motor capabilities to guide the robot while carrying heavy loads in a reliable and comfortable way by considering his intention. To achieve these goals, a robotic structure is built as shown in Fig. 1, which illustrates the diagram of the human–robot interaction, implemented with a Pioneer 3AT robot and a bar mounted on it. The bar will be maneuvered by a human to indicate the motion intention to the robot control. The

Fig. 1 System: **a** human–robot interaction; **b** robotic system developed

(a) Human-Robot interaction **(b)** Robotic system developed

desired human orientation is detected by a sensor (sensor 3) located at the base of the bar as shown in Fig. 1b.

The main goal is to maneuver the robot with minor effort during all interactions; therefore, it is necessary to sense the human force on the robot. Hence, two force sensors have been incorporated to the bar (sensors 1 and 2 in Fig. 1b), one for detecting the push force f_{Ht} and the other for the pull force f_{Hr} to control the movement of the robot, forward or backward, respectively, and the resultant force being $f_H = f_{Ht} - f_{Hr}$ (Fig. 2). Additionally, the system includes a laser range sensor (0°–180°) to detect and avoid obstacles during the interaction.

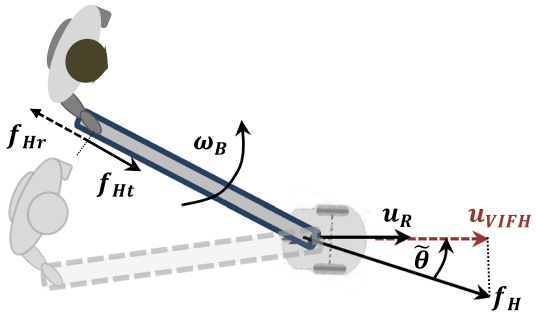

Fig. 2 Human–robot interaction diagram

3 Modeling of interaction forces

3.1 Modeling of the velocity induced by the human force u_{VIFH}

The human force is sensed to allow the person to maneuver the robot in an easy and comfortable way through the environment. Additionally, it is important that the person feels some slight inertia of the system during the interaction. So, the velocity induced by the human force (u_{VIFH}) in the human desired direction is modeled using a mechanical impedance reference Z_h, with a mass M_h and damping D_h, as:

$$u_{\mathrm{VIFH}} = {Z_h}^{-1} f_H \cos\tilde{\theta} = \frac{1}{(M_h s + D_h)} f_H \cos\tilde{\theta}, \qquad (1)$$

where $\tilde{\theta}$ is the angle error between the robot orientation and the desired orientation defined by the human. Also, in Fig. 2, u_R is the robot linear velocity. Moreover, when the human changes the orientation reference, an angular velocity ω_B is generated over the bar which must be estimated since it is required by the robot controller.

As a graphic example of the model behavior, Fig. 3 shows the evolution of u_{VIFH} under changes on M_h and D_h for a constant $f_H = 1$ and $\tilde{\theta} = 0$. It can be noted that when M_h decreases (being $D_h = 1$ for Fig. 3), the convergence time of u_{VIFH} also decreases. This behavior is because the system is modeled with less mass and presents therefore less inertia when there is a change in the reference force.

On the other hand, if $D_h < 1$, the effect of an augmented force applied to u_{VIFH} is produced, implying less effort to carry loads. Parameters M_h and D_h were determined experimentally by taking into account both the human comfort and the control errors.

In this work, human comfort is associated with the physical user's ability of carrying loads. Therefore, for healthy users without motor disorders, parameters setting can be made by giving some priority to the navigation performance. On the other hand, when the user is an elderly or handicapped person, the navigation performance should be relaxed allowing the person to comfortably use the proposed robotic device. This way, human comfort is determined by performing contextual interviews to the users, which are combined with the observation of navigation performance to determine the most appropriate parameter set for each user.

3.2 Modeling of the environment interaction force

Since the human–robot interaction can take place in unstructured environments, it is necessary to implement an obstacle avoidance strategy. The proposed strategy generates a circular repulsion zone around the robot (as Fig. 4 shows) regardless of the obstacle size or shape. This is a desired situation, especially when the robot interacts in complex environments with humans.

Then, a Gaussian zone is created within the repulsion zone, giving greater importance to the obstacles placed directly in front of the robot when compared with those obstacles found on the sides. This new zone allows the user, for example, to guide the robot through narrow or crowded corridors. When obstacles are located within the repulsion zone (bounded by the distance d_L), a normal fictitious force is generated in the opposite direction with respect to the robot movement and a

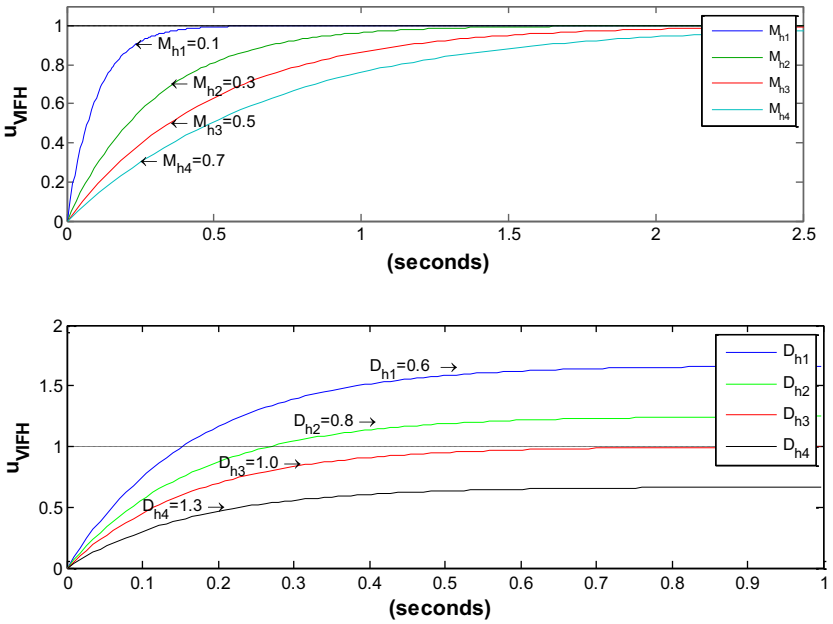

Fig. 3 Evolution of u_{VIFH} for different M_h and D_h values

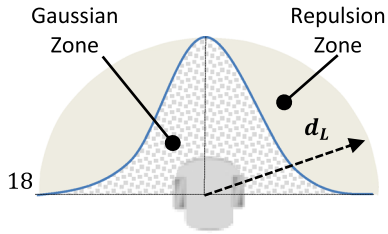

Fig. 4 Zones to detect obstacles

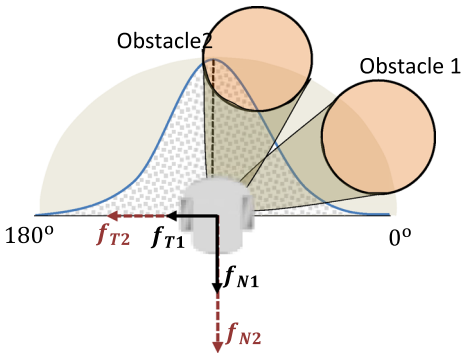

Fig. 5 Forces f_N and f_T for two different obstacles

fictitious tangential force is used to generate a new reference orientation which aims to avoid the obstacles. Figure 5 shows how f_N and f_T are larger when the obstacle is in front of the robot than in the case when the obstacle is on its side.

Forces f_N and f_T are computed as:

$$f_N = \frac{1}{f_{N_{\max}}} \sum_{i=0}^{n=180} f_o(i) \sin(i) \tag{2}$$

$$f_T = \frac{1}{f_{T_{\max}}} \sum_{i=0}^{n=180} f_o(i) \cos(i) \tag{3}$$

$$u_{\text{obj}} = {D_N}^{-1} f_N \tag{4}$$

$$\omega_{\text{obj}} = k_\psi \tanh(f_T), \tag{5}$$

where ω_{obj} is the obstacle reference angular velocity and u_{obj} is the obstacle reference linear velocity, which are applied to the robot to avoid the obstacle, k_ψ is a positive constant for matching force units to angular velocity; D_N is a positive constant of damping to match u_{obj} with input f_N. Variable f_o is the environment force defined as:

$$f_o(i) = y_g(i) f_m(i); \quad 0° \leq i \leq 180°, \tag{6}$$

where $f_m(i)$ represents the fictitious force generated by the environment, y_g is a Gaussian function defined by:

$$y_g(i) = e^{-\left(\frac{x(i)-x_m}{\sigma}\right)^2}, \tag{7}$$

with x_m being the medium laser line (in this case, 90°), σ is the standard deviation of the Gaussian distribution to calibrate the width of the Gaussian area, and $x(i)$ is the laser line of each angle (from 0° to 180°). It is important to note that σ is selected by considering the physical dimension of the robotic device, and it is set as the smallest value that allows the robot to pass through between two close obstacles safely. Fictitious force $f_m(i)$ is calculated as follows [27]:

$$f_m(i) = Z_m \tilde{x}(i) = \left(M_m s^2 + D_m s + K_m\right) \tilde{x}(i), \tag{8}$$

where $\tilde{x}(i) = (d_{\text{obj}}(i) - d_L)$; Z_m is mechanical impedance; M_m, D_m, and K_m are the parameters for mass, damping, and

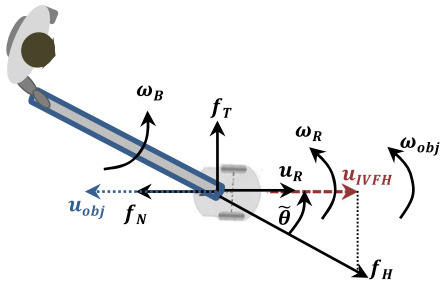

Fig. 6 System control variables

elasticity, respectively. The variable $d_{\text{obj}}(i)$ is the distance between the objects and the robot for each laser line within the repulsion zone. After modeling the forces, in the next section the design of the controllers is presented .

4 Controllers

4.1 Kinematic controller

As previously mentioned, the control objective is to allow the human to guide the robot at the desired velocity with the desired orientation. The robot must also react accordingly to the human intention in the presence of obstacles.

Figure 6 shows the bilateral interaction system with its kinematics defined by:

$$\tilde{u} = u_{\text{VIFH}} - u_R - u_{\text{obj}} \tag{9}$$

$$\dot{\tilde{\theta}} = \omega_B - \omega_R - \omega_{\text{obj}}, \tag{10}$$

where $\tilde{u}$ is the velocity error, $\dot{\tilde{\theta}}$ is the time derivative of the robot orientation error, u_R and ω_R are the linear and the angular velocities of the robot, respectively, and u_{obj} and ω_{obj} are the linear and the angular velocities generated to avoid obstacles ((4) and (5), respectively). Now, as defined in the previous Section, $\tilde{u}$ is expressed as $\tilde{u} = \mathrm{d}\dot{\tilde{\rho}}/\mathrm{d}t = \ddot{\tilde{\rho}}$, with $\tilde{\rho}$ being an auxiliary variable. Then, the kinematics can be rewritten as:

$$\dot{\tilde{\rho}} = u_{\text{VIFH}} - u_R - u_{\text{obj}} \tag{11}$$

$$\dot{\tilde{\theta}} = \omega_B - \omega_R - \omega_{\text{obj}}. \tag{12}$$

The proposed kinematic control laws are:

$$u_{R_C} = u_{\text{VIFH}} + q_\rho \tanh\left(\frac{k_\rho\,\tilde{\rho}}{q_\rho}\right) - u_{\text{obj}} \tag{13}$$

$$\omega_{R_C} = \omega_B + q_\omega \tanh\left(\frac{k_\omega\,\tilde{\theta}}{q_\omega}\right) - \omega_{\text{obj}}, \tag{14}$$

where k_ρ, k_ω, q_ρ, and q_ω are positive constants. Next, we introduce a Lyapunov candidate function and its time derivative on the system trajectories to analyze the equilibrium point's stability:

$$V\left(\tilde{\theta}, \tilde{\rho}\right) = \tilde{\rho}^2/2 + \tilde{\theta}^2/2, \tag{15}$$

$$\dot{V}(\tilde{\theta}, \tilde{\rho}) = \tilde{\rho}\,\dot{\tilde{\rho}} + \tilde{\theta}\,\dot{\tilde{\theta}},$$
$$\dot{V}(\tilde{\theta}, \tilde{\rho}) = \tilde{\rho}\,(u_{\text{VIFH}} - u_R - u_{\text{obj}} + \tilde{\theta}\,(\omega_B - \omega_R - \omega_{\text{obj}}). \tag{16}$$

Now, by replacing the control laws (13) and (14) under the assumption of perfect velocity tracking (i.e., $u_R \equiv u_{R_C}$ and $\omega_R \equiv \omega_{R_C}$), the time derivative $\dot{V}$ is:

$$\dot{V}(\tilde{\theta}, \tilde{\rho}) = -\tilde{\rho}\; q_\rho \tanh\left(\frac{k_\rho\,\tilde{\rho}}{q_\rho}\right) - \tilde{\theta}\; q_\omega \tanh\left(\frac{k_\omega\,\tilde{\theta}}{q_\omega}\right). \tag{17}$$

Note that the function $\tanh(\tilde{x})$ is a bounded continuous saturation function applied to the error, such that $\tilde{x}\tanh(\tilde{x}) > 0$. Then $\dot{V} < 0$, thus concluding that $\tilde{\rho} \to 0$ and $\tilde{\theta} \to 0$ asymptotically. Moreover, knowing that $\tilde{u} = u_{\text{VIFH}} - u_R - u_{\text{obj}}$ and including the control action in (9): $\tilde{u} = -q_\rho \tanh(k_\rho\,\tilde{\rho}/q_\rho)$. As was previously proved that $\tilde{\rho} \to 0$ with $t \to \infty$, it immediately follows that $\tilde{u} \to 0$ asymptotically.

As mentioned, the above analysis is based on the perfect velocity tracking assumption ($\mathbf{v} = \mathbf{v}_C$ for all t), with $\mathbf{v}_C = [u_C \quad \omega_C]^{\mathrm{T}}$ and $\boldsymbol{\nu} = [u_R \quad \omega_R]^{\mathrm{T}}$. However in a real situation, the robot velocity is not identical to the kinematics controller velocity and thus $\mathbf{v} - \mathbf{v}_C = \boldsymbol{\delta}$, with the velocity error vector being $\boldsymbol{\delta} = [\delta_\rho \quad \delta_\omega]^{\mathrm{T}}$. Considering now the linear and angular velocity errors, the resulting closed-loop equations are:

$$\dot{\tilde{\rho}} = -q_\rho \tanh\left(\frac{k_\rho\,\tilde{\rho}}{q_\rho}\right) + \delta_\rho \tag{18}$$

$$\dot{\tilde{\theta}} = -q_\omega \tanh\left(\frac{k_\omega\,\tilde{\theta}}{q_\omega}\right) + \delta_\omega \tag{19}$$

Considering the following Lyapunov candidate function and its time derivative in the trajectories of the system:

$$V_1 + V_2 = \frac{\tilde{\rho}^2}{2} + \frac{\tilde{\theta}^2}{2}, \tag{20}$$

$$\dot{V}_1 + \dot{V}_2 = \tilde{\rho}\,\dot{\tilde{\rho}} + \tilde{\theta}\,\dot{\tilde{\theta}}, \tag{21}$$

$$\dot{V}_1 = -\tilde{\rho}\; q_\rho \tanh\left(\frac{k_\rho\,\tilde{\rho}}{q_\rho}\right) + \tilde{\rho}\,\delta_\rho, \tag{22}$$

$$\dot{V}_2 = -\tilde{\theta}\, q_\omega \tanh\left(\frac{k_\omega\,\tilde{\theta}}{q_\omega}\right) + \tilde{\theta}\,\delta_\omega, \tag{23}$$

it can be seen from (22) that a sufficient condition for $\dot{V}_1$ to be negative definite is

$$\left|\left|\tilde{\rho}\ q_\rho\ \tanh\left(\frac{k_\rho \tilde{\rho}}{q_\rho} q_\rho\right)\right|\right| > \left|\left|\tilde{\rho}\ \delta_\rho\right|\right|. \tag{24}$$

Now, by making a similar analysis as in [28], for large values of $\tilde{\rho}$, the condition (24) can be reinforced as:

$$\left|\left|\tilde{\rho}\ q_{\rho L}\right|\right| > ||\tilde{\rho}||\ \left|\left|\delta_\rho\right|\right|, \tag{25}$$

where $q_{\rho L} < q_\rho$, such that $q_{\rho L} = q_\rho \tanh(k_{N\rho})$ and $k_{N\rho}$ is a suitable positive constant (see Fig. 7). Then, $\dot{V}_1$ will be negative definite if:

$$\left|\left|q_\rho\right|\right| > \frac{||\delta_\rho||}{\tanh(k_{N\rho})}. \tag{26}$$

Equation (26) defines a design condition to make the error $\tilde{\rho}$ decrease. Now, for small values of $\tilde{\rho}$, the condition (24) will be fulfilled if (see Fig. 7)

$$\left|\left|\tilde{\rho}^2\ k_\rho\ \tanh(k_{N\rho}) \Big/ k_{N\rho}\right|\right| > \left|\left|\tilde{\rho}\ \delta_\rho\right|\right|. \tag{27}$$

Therefore, a sufficient condition for $\dot{V}_1$ to be negative definite is:

$$||\tilde{\rho}|| > \frac{k_{N\rho}||\delta_\rho||}{k_\rho\ \tanh(k_{N\rho})}. \tag{28}$$

Then, the $\tilde{\rho}$ is ultimately bounded by:

$$||\tilde{\rho}|| \leq \frac{k_{N\rho}||\delta_\rho||}{\xi\ k_\rho\ \tanh(k_{N\rho})}; \quad 0 < \xi < 1. \tag{29}$$

Moreover, knowing that $\tilde{u} = \dot{\tilde{\rho}}$, then $\tilde{u} = -q_\rho\ \tanh(k_\rho\ \tilde{\rho}/q_\rho) + \delta_\rho$. Therefore, $\tilde{u}$ is ultimately bounded by:

$$||\tilde{u}|| \leq \left|\left|-q_\rho\ \tanh\left(\frac{k_{N\rho}||\delta_\rho||}{\xi\ q_\rho\ \tanh\left(k_{N\rho}\right)}\right) + \delta_\rho\right|\right|. \tag{30}$$

The diagram in Fig. 7 illustrates the saturation function and its lower bound considered in the analysis.

Performing a similar analysis for $\dot{V}_2$, it is possible to conclude that a sufficient condition for $\dot{V}_2$ to be negative definite is:

$$||\tilde{\theta}|| > \frac{k_{N\omega}||\delta_\omega||}{k_\omega\ \tanh(k_{N\omega})}. \tag{31}$$

Then, $\tilde{\theta}$ is ultimately bounded by:

$$||\tilde{\theta}|| \leq \frac{k_{N\omega}\delta_\omega}{\xi\ k_\omega\ \tanh\left(k_{N\omega}\right)}; \quad 0 < \xi < 1. \tag{32}$$

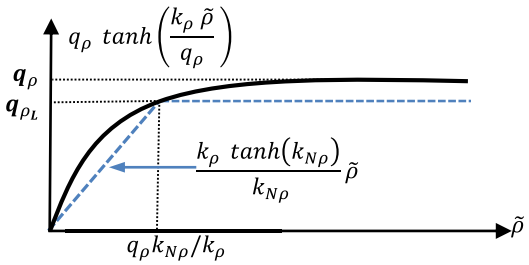

Fig. 7 Diagram of the lower bound for the saturation function

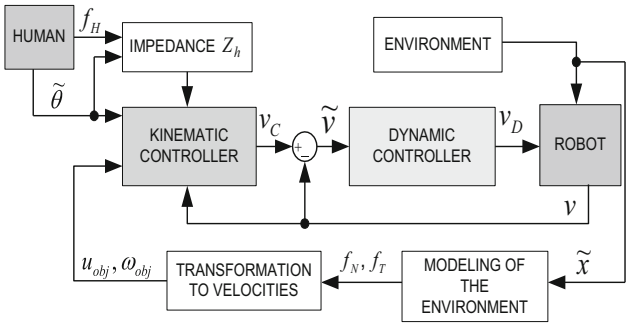

Fig. 8 Control system diagram

However, as previously proved: $u_R \to u_c$ and $\omega_R \to \omega_c$ with $t \to \infty$. Then, $\delta_\rho(t) \to 0$ and $\delta_\omega(t) \to 0$ with $t \to \infty$ and it is finally concluded that $\tilde{u} \to 0$ and $\tilde{\theta} \to 0$ asymptotically. Therefore, the control objective is attained.

4.2 Dynamic controller

As said in the previous section, kinematic control laws do not allow to exactly match the robot velocity due to the robot dynamics. A velocity error appears $\mathbf{v}_C - \mathbf{v} = \tilde{\mathbf{v}}$, with $\mathbf{v}_C = [u_C \quad \omega_C]^{\mathrm{T}}$ and $\mathbf{v} = [u_R \quad \omega_R]^{\mathrm{T}}$. The goal of the dynamic controller design is to compensate the robot dynamics by introducing a cascade block to generate a new reference velocity for the robot: $\mathbf{v}_D = [u_D \quad \omega_D]^{\mathrm{T}}$. Figure 8 shows the complete control diagram, including the dynamic compensation controller which is designed in the following.

The robot dynamic model is defined by

$$\mathbf{M}\dot{\mathbf{v}} + \boldsymbol{\eta} = \mathbf{v}_D, \tag{33}$$

$$\boldsymbol{\eta} = \begin{bmatrix} 0 & 0 & -\omega_R{}^2 & u_R & 0 & 0 \\ 0 & 0 & 0 & 0 & u_R\omega_R & \omega_R \end{bmatrix} \boldsymbol{\phi}, \tag{34}$$

$$\boldsymbol{\phi} = [\phi_1 \quad \phi_2 \quad \phi_3 \quad \phi_4 \quad \phi_5 \quad \phi_6]^{\mathrm{T}}, \tag{35}$$

$$\mathbf{M} = \begin{bmatrix} \phi_1 & 0 \\ 0 & \phi_2 \end{bmatrix}, \tag{36}$$

where ϕ_1, ϕ_2, ϕ_3, ϕ_4, ϕ_5, and ϕ_6 are the identified parameters for the Pioneer 3AT robot ($\phi_1 = 0.4072$, $\phi_2 = 0.2937$, $\phi_3 = -0.0287$, $\phi_4 = 0.9979$, $\phi_5 = -0.0004$, and $\phi_6 = 0.9865$)

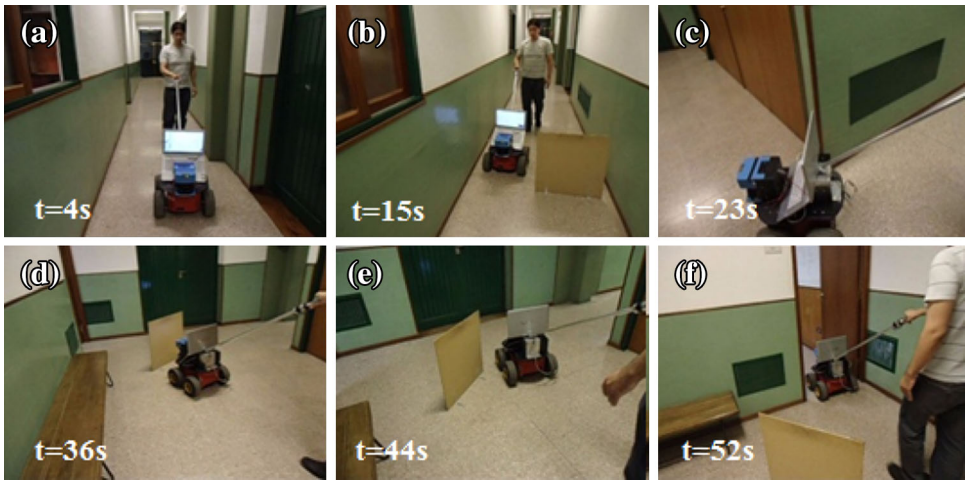

Fig. 9 Environment and sequence of the experiment

[29]. The proposed dynamic control law is defined as:

$$\mathbf{v}_D = \mathbf{M}\boldsymbol{\sigma} + \boldsymbol{\eta} \tag{37}$$

such that:

$$\boldsymbol{\sigma} = \dot{\mathbf{v}} + \mathbf{Q}_D \tanh(\mathbf{Q}_D^{-1}\, \mathbf{K}_D\, \tilde{\mathbf{v}}), \tag{38}$$

where $\mathbf{Q}_D$ and $\mathbf{K}_D$ are positive definite symmetric matrices. The closed loop equation when replacing (37) in (33) is $\dot{\tilde{\mathbf{v}}} + \mathbf{Q}_D \tanh(\mathbf{Q}_D^{-1}\, \mathbf{K}_D\, \tilde{\mathbf{v}}) = \mathbf{0}$, with $\tilde{\mathbf{v}} = \dot{\mathbf{v}}_C - \dot{\mathbf{v}}$. Next, a Lyapunov candidate function with its time derivative is considered:

$$V(\tilde{v}) = \frac{1}{2}\tilde{\mathbf{v}}^{\mathrm{T}}\tilde{\mathbf{v}}, \tag{39}$$

$$\dot{V}(\tilde{v}) = \tilde{\mathbf{v}}^{\mathrm{T}}\,\dot{\tilde{\mathbf{v}}}, \tag{40}$$

$$\dot{V}(\tilde{v}) = -\tilde{\mathbf{v}}^{\mathrm{T}}\big[\mathbf{Q}_D \tanh(\mathbf{Q}_D^{-1}\, \mathbf{K}_D\, \tilde{\mathbf{v}})\big]. \tag{41}$$

Remembering that $\mathbf{Q}_D$ and $\mathbf{K}_D$ are positive definite symmetric diagonal matrices, and the function $\tanh(\tilde{\mathbf{v}})$ is a bounded saturation continuous function applied to the velocity error, such that $\tilde{\mathbf{v}}^{\mathrm{T}} \tanh(\tilde{\mathbf{v}}) > 0$, it can be concluded that $\dot{V} < 0$, allowing to prove that $\tilde{\mathbf{v}} \to \mathbf{0}$ asymptotically.

5 Experimental results

The proposed control algorithm was implemented in the robotic system shown in Fig. 1. The force sensor range is $100N$. The measured variables, force and $\tilde{\theta}$ angle, are filtered by an α-β-γ filter [30], obtaining the estimates of $\dot{\tilde{\theta}}$ used to calculate ω_B (8). In the proposed experiment, the person guides the robot along a corridor with two obstacles before passing through a standard door. The first experimental results had presented oscillations and high control error; so, parameters M_h and D_h were experimentally set to reduce

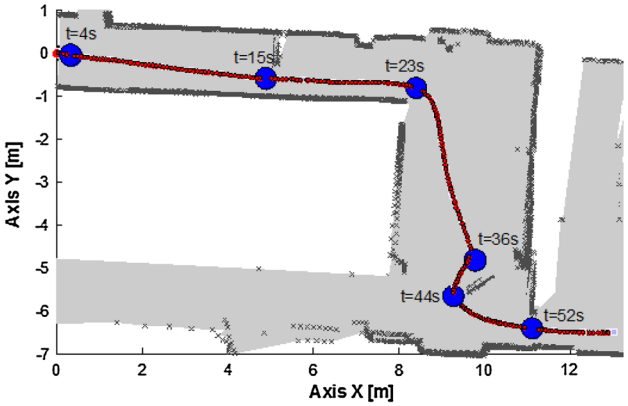

Fig. 10 Sequence of the experiment

oscillations and control errors, but also taking into account the human comfort. In addition, an alpha–beta–gamma filter was implemented to get the data from the sensors, thereby significantly decreasing the oscillations.

The environment impedance parameters were defined as $M_m = 0.01$, $D_m = 0.1$, and $K_m = 1$. On the other hand, for modeling of u_{VIFH}, the impedance parameters were selected as $M_h = 0.1$ and $D_h = 1$. The kinematic controller parameters were set to: $k_\rho = 0.5$; $q_\rho = 0.4$; $k_\omega = 0.6$; $q_\omega = 1.5$. The dynamic controller parameters were set to: $\mathbf{Q_D} = [0.8 \;\; 0;\; 0 \;\; 0.8]$; $\mathbf{K_D} = [2.8 \;\; 0;\; 0 \;\; 1.8]$. Figure 9 shows an images sequence of the experiment, which can be related to the map in Fig. 10

Figure 11 shows the evolution of the forces f_{Ht} and f_{Hr}. These forces represent the human intention so that the robot moves forward or backward, respectively. They are also critical to facilitate humans to maneuver and translate the robot through narrow areas.

Figure 12 shows the time evolution of u_{VIFH} (solid line) and f_H (dashed line) normalized to the maximum robot velocity. The difference between u_{VIFH} and f_H for a change

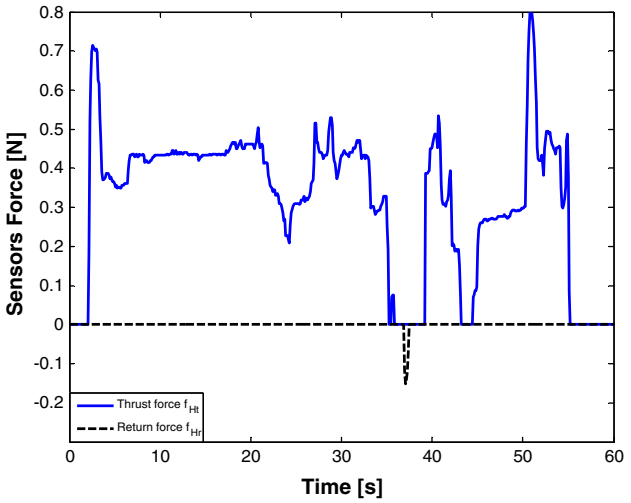

Fig. 11 Evolution of thrust force f_{Ht} and return force f_{Hr}

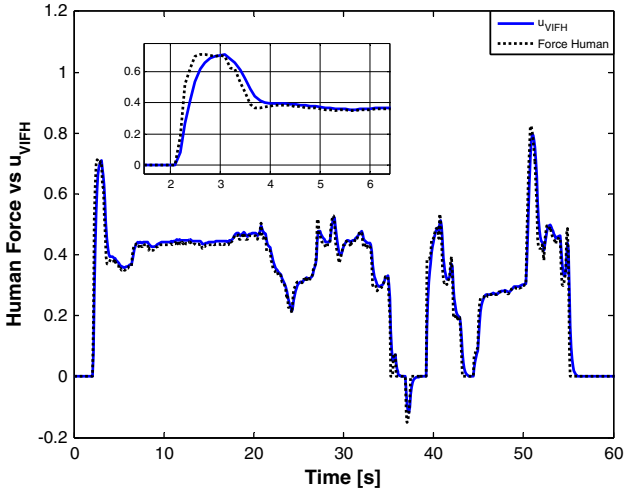

Fig. 12 Evolution of u_{VIFH} and the human force f_H

of reference can be seen in the upper box in Fig. 12. M_h and D_h can be calculated for greater human comfort, but at the price of increasing the control error. Therefore, it is necessary to look for a balance between human comfort and the control error. Figure 13 shows the time evolution of u_{VIFH} (solid line), u_R (dotted line), and normal force f_N (dashed line), with the latter normalized to the maximum robot velocity. When the human applies f_H on the robot at $t = 3\,\text{s}$, a transient difference appears between u_R and u_{VIFH} corresponding to the robot inertia. Then, the robot reaches the reference velocity $u_R \rightarrow u_{\text{VIFH}}$. From $t = 11\,\text{s}$ to $t = 22\,\text{s}$, a force f_N appears due to the presence of the first obstacle. As the human moves alongside the object, the f_N generated is small due to the features of the obstacle avoidance strategy with the Gaussian zone. From $t = 32\,\text{s}$ to $t = 38\,\text{s}$ when the person deliberately tries to crash with the second obstacle (for the system evaluation purposes only), a fictitious force f_N is observed, which opposes the robot movement. At this moment, u_R cannot converge to u_{VIFH} as expected. The same occurs when the person passes through the door at $t = 50\,\text{s}$ to $t = 54\,\text{s}$.

Figure 14 shows the $\tilde{u}$ error, whereas Fig. 15 shows the $\tilde{\theta}$ error. Notice that $\tilde{u}$ increases when there is an obstacle or when the reference force changes abruptly. In Fig. 15, the increase in error $\tilde{\theta}$ from $t = 21\,\text{s}$ to $t = 28\,\text{s}$ is due to the appearance of a corner in the hallway (Fig. 9c). Also, the error increases from $t = 38\,\text{s}$ to $t = 50\,\text{s}$ while the person avoids the second obstacle and passes through the door. From the experiment, we can understand the good performance of the proposed control algorithm, with the experimental control errors remaining bounded within acceptable values.

Finally, the effect of the Gaussian zone of the obstacle avoidance strategy is analyzed in the experiment. Figure 16 shows the evolution of the normal force f_N with and with-

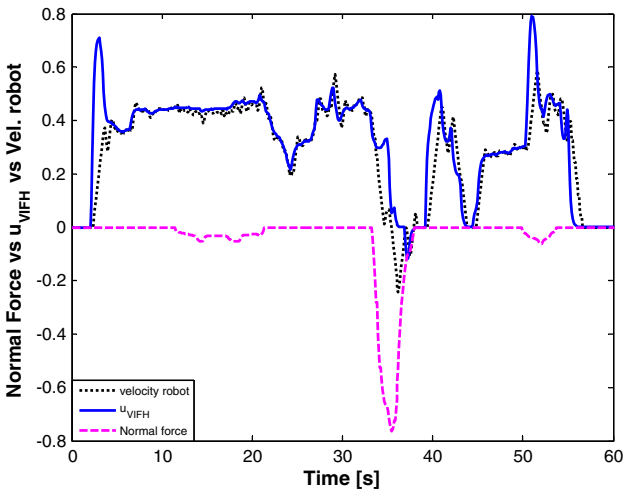

Fig. 13 Evolution of u_{VIFH}, u_R, and f_N

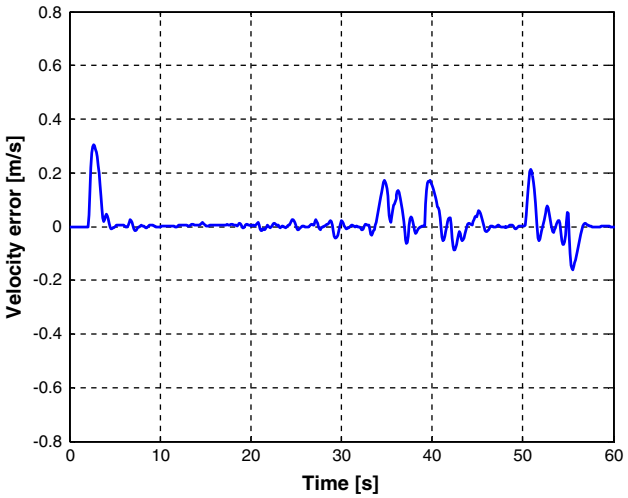

Fig. 14 Evolution of speed error $\tilde{u}$

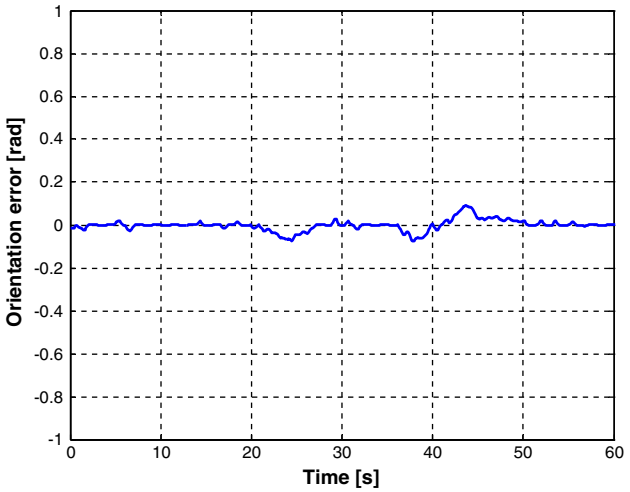

Fig. 15 Evolution of orientation error $\tilde{\theta}$

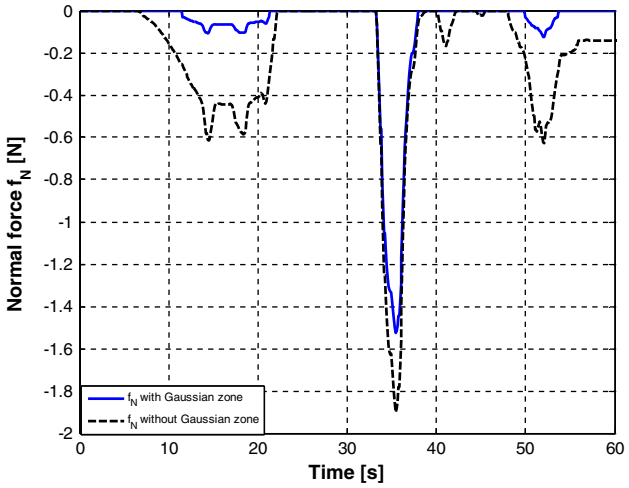

Fig. 16 Evolution of normal force f_N with and without the Gaussian zone

out the Gaussian zone. A normal force appears at $t = 7\,\text{s}$ and up to $t = 22\,\text{s}$ without the Gaussian zone (dashed line). This force is larger than the normal force with the Gaussian zone (continuous line) at $t = 11\,\text{s}$ up to $t = 21\,\text{s}$. The force is generated due to the presence of the first obstacle in the corridor as shown in Fig. 9b. This force opposes the robot movement; however, the aim is that humans can overcome the obstacle with the robotic system. Thus, the consideration of the Gaussian zone is very important when the human intends to go through a narrow area. The same occurs from $t = 48\,\text{s}$ to $t = 60\,\text{s}$ where the human intends to go through the door (Fig. 9f). Starting at $t = 32\,\text{s}$ and up to $t = 39\,\text{s}$, the human intends to crash with the second obstacle. In this case, the force (with or without Gaussian zone) is large enough to prevent this crash (Fig. 9d).

The same happens with the tangential force f_T as shown in Fig. 17. This force is generated due to the presence of obstacles. The f_T is larger without the Gaussian zone than that with Gaussian zone from $t = 7\,\text{s}$ to $t = 22\,\text{s}$ and from $t = 48\,\text{s}$ to $t = 60\,\text{s}$. At $t = 34\,\text{s}$ and up to $t = 39\,\text{s}$, the tangential force f_T prevents the robot from crashing with the obstacle. This force becomes relevant as it helps the human to avoid obstacles by adding a component to the human intention, allowing the person to easily guide the robot through narrow or crowded corridors.

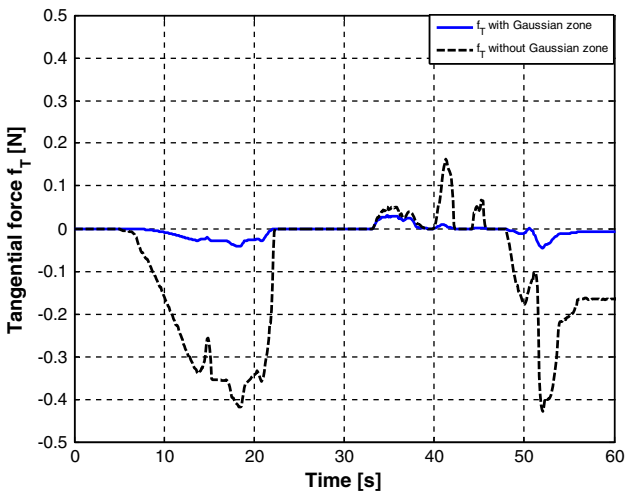

Fig. 17 Evolution of tangential force f_T with and without the Gaussian zone

6 Conclusions

In this work, an interactive human–robot system was developed to be applied in tasks such as carrying loads, guiding persons, or moving the robot along any unstructured environment easily and comfortably. The authors studied the robot motion control based on the human intention to guide the robot. The main contribution of this work has been to present a control algorithm based on bilateral human–robot interaction, designed to help a person with reduced strength and elderly or children to carry heavy loads with minimal effort in unstructured environments. Additionally, the proposed system can be used for guiding visually impaired people to detect and avoid obstacles. It includes a formal analysis of stability of the control system based on Lyapunov theory. The good performance of this control strategy has been shown through real experimental results. Future work is expected to analyze the robustness of the algorithm with estimated errors, and the design of adaptive controllers for significant charges in the load carried by the robot.

Acknowledgements Funding was provided by Universidad Nacional de San Juan (AR), Consejo Nacional de Investigaciones Científicas y Técnicas, Fondo para la Investigación Científica y Tecnológica.

References

1. Lam CP, Chou CT, Chiang KH, Fu LC (2011) Human-centered robot navigation—towards a harmoniously human–robot coexisting environment. IEEE Trans Robots 27(1):99–112
2. Tsai C, Dutoit X, Song K, Van Brussel H, Nuttin M (2010) Robust face tracking control of a mobile robot using self-tuning Kalman filter and echo state network. Asian J Control 12(4):488–509
3. Leica P, Toibero JM, Roberti F, Carelli R (2015) Switched control to robot–human bilateral interaction for guiding people. J Intell Robot Syst 77(1):73–93
4. Ulrich I, Borenstein J (2001) The guidecane: applying mobile robot technologies to assist the visually impaired. IEEE Trans Syst Man Cybern Part A Syst Hum 31(2):131–136
5. Hirata Y, Ojim Y, Kosuge K (2008) Variable motion characteristics control of an object by multiple passive mobile robots in cooperation with a human. In: Proceedings of IEEE international conference on robotics and automation, pp 1346–1351, Pasadena CA, USA
6. Wang Z, Fukaya K, Hirata Y, Kosuge K (2007) Control of passive mobile robots for object transportation—braking torque analysis and motion control. In: Proceedings of IEEE international conference on robotics and automation, pp 2874–2879, Roma, Italy
7. Hirata Y, Song H, Wang Z, Kosgue K (2007) Control of passive object handling robot with free joint for reducing human assistive force. In: Proceedings of IEEE/RSL international conference on intelligent robots and systems, pp 1154–1159, San Diego CA, USA
8. Manuel J, Wandosell H, Graf B (2002) Non-holonomic navigation system of awalking-aid robot. In: Proceedings of IEEE international workshop on robot and human interactive communication, pp 518–523, Berlin, Germany
9. Hirata Y, Hara A, Kosuge K (2007) Motion control of passive intelligent walker using servo brakes. IEEE Trans Robot 23(5):981–990
10. Yu H, Spenko M, Dubowsky S (2003) An adaptive shared control system for an intelligent mobility aid for the elderly. Auton Robots 15(1):53–66
11. Roy N, Baltus G, Fox D, Gemperle F, Goetz J, Hirsch T, Margaritis D (2000) Towards personal service robots for the elderly. In: Proceedings of workshop interactive robotics and entertainment, Pittsburgh PA, USA
12. Garcia F, Bartolini F, Frizera R (2010) Object transportation task by a human and a mobile robot. IEEE international conference on industrial technology (ICIT), pp 1445–1450
13. Hirata Y, Ojima Y, Kosuge K (2007) Handling of an object in 3D space by multiple mobile manipulators based on intentional force/moment applied by human. In: Proceedings of IEEE/ASME international conference on advanced intelligent mechatronics, pp 1–6, Zürich, Switzerland
14. Hirata Y, Kume Y, Wang Z, Kosuge K (2003) Decentralized control of multiple mobile manipulators based on virtual 3-D caster motion for handling an object in cooperation with a human. In: Proceedings of IEEE international conference on robotic & automation, Taiwan
15. Wakita W, Huamg J, Di P, Sekiyama K, Fukuda T (2013) Human-walking-intention-based motion control of an omnidirectional-type cane robot. IEEE/ASME Trans Mechatron 18:285–296
16. Ferland F, Aumont A, Létourneau D, Michaud F (2013) Taking your robot for a walk: force-guiding a mobile robot using compliant arms. In: Proceedings of ASM/IEEE international conference on human–robot interaction, pp 309–316, Tokyo, Japan
17. Nagarajan U, Kantor G, Hollis R (2009) Human–robot physical interaction with dynamically stable mobile robots. In: Proceedings of ACM/IEEE international conference on human–robot interaction, pp 281–282, La Jolla CA, USA
18. Abidi S, Williams M, Johnston B (2013) Human pointing as a robot directive. In: Proceedings of ACM/IEEE international conference on human–robot interaction, pp 67–68, Tokyo, Japan
19. Chuy O, Hirata Y, Kosuge K (2006) A new control approach for a robotic walking support system in adapting user characteristics. IEEE Trans Syst Man Cybern 36:725–733
20. Yamada Y, Umetani Y, Daitoh H, Sakai T (1999) Construction of a human/robot coexistence system based on a model of human will-intention and desire. In: Proceedings of IEEE international conference on robotics and automation, pp 2861–2867, Detroit MI, USA
21. Huang J, Di P, Fukuda T, Matsuno T (2008) Motion control of omnidirectional-type cane robot based on human intention. In: Proceedings of IEEE/RSJ international conference on intelligent robots and systems, pp 273–278, Nice, France
22. Garcia D, Slawinsky E, Mut V (2013) Collaborater for a car-like vehicle driven by a user with visual inattention. Asian J Control 15:177–192
23. Mori H, Kotani S (1998) A robotic travel aid for the blind—attention and custom for safe behavior. In: Proceedings of international symposium of robotics research, pp 237–254, Shonan, Japan
24. Hirata Y, Muraki A, Kosuge K (2006) Motion control of intelligent passive-type walker for fall-prevention function based on estimation of user state. In: Proceedings of IEEE international conferences on robotics and automation, pp 3498–3503, Orlando FL, USA
25. Kosuge K, Hayashi T, Hirata Y, Tobiyama R (2003) Dance partner robot:Ms DanceR. In: Proceedings of IEEE/RSJ international conference on intelligent robots and systems, pp 3459–3464, LasVegas NV, USA
26. Takeda T, Hirata Y, Kosuge K (2007) Dance step estimation method based on HMM for dance partner robot. IEEE Trans Ind Electron 54(2):699–706
27. Secchi H, Carelli R, Mut V (2003) An experience on stable control of mobile robots. Lat Am Appl Res 33(4):379–386
28. Andaluz V, Roberti F, Toibero JM, Carelli R (2012) Adaptive unified motion control of mobile manipulators. Control Eng Pract 20(12):1337–1352
29. Andaluz V, Roberti F, Toibero JM, Carelli R, Wagner B (2011) Adaptive dynamic path following control of an unicycle-like mobile robot. In: Proceedings of international conference on intelligent robotics and applications, Aachen, Germany
30. Kalata P (1984) The tracking index: a generalized parameter for $\propto$–β and $\propto$–β–γ target trackers. IEEE Trans Aerosp Electron Syst 20(2):174–182